

# Resonant instabilities of kinetic Alfvén waves in the Earth's magnetosphere with superthermal electrons

Cite as: Phys. Plasmas **26**, 112108 (2019); doi: [10.1063/1.5114907](https://doi.org/10.1063/1.5114907)

Submitted: 12 June 2019 · Accepted: 16 October 2019 ·

Published Online: 7 November 2019



View Online



Export Citation



CrossMark

K. C. Barik,<sup>a)</sup>  S. V. Singh,<sup>b)</sup>  and G. S. Lakhina<sup>c)</sup> 

## AFFILIATIONS

Indian Institute of Geomagnetism, Navi Mumbai 410218, India

<sup>a)</sup>Electronic mail: [kcbarik16@iigs.iigm.res.in](mailto:kcbarik16@iigs.iigm.res.in)

<sup>b)</sup>Electronic mail: [satyavir@iigs.iigm.res.in](mailto:satyavir@iigs.iigm.res.in)

<sup>c)</sup>Electronic mail: [gslakhina@gmail.com](mailto:gslakhina@gmail.com)

## ABSTRACT

A theoretical plasma model for the generation of kinetic Alfvén waves (KAWs), having background Maxwellian ions,  $\kappa$ -electrons, and drifting Maxwellian beam ions, is discussed. The ion beam streams along the ambient magnetic field, whereas velocity shear is perpendicular to it. The role played by nonthermal electrons in the excitation of resonant KAWs with the velocity shear in the ion beam as the free energy source is examined. In the presence of  $\kappa$ -electrons, the effect of plasma parameters such as propagation angle, ion beam temperature, number density, and ion plasma  $\beta_i$  on the growth of the KAWs is analyzed. It is found that nonthermal electrons restrict the excitation of KAWs by reducing the growth rate of the waves. It is inferred that a high velocity shear and ion beam density are required to excite KAWs in the presence of nonthermal electrons. The model is capable of producing waves with frequencies up to  $\approx 18$  mHz in the auroral region of Earth's magnetosphere.

Published under license by AIP Publishing. <https://doi.org/10.1063/1.5114907>

## I. INTRODUCTION

Kinetic Alfvén Waves (KAWs) are ultralow frequency (ULF) waves in the range of  $\approx (0-30)$  Hz having nearly perpendicular propagation to the ambient magnetic field. These waves play a vital role in particle energization and auroral electron acceleration because of the presence of parallel electric field.<sup>1,2</sup> The parallel electric field arises due to finite ion gyroradius or electron inertial length. The kinetic effect comes into the picture under two conditions: for the hot electron case, the effect comes into play when the perpendicular wavelength is comparable to the ion gyroradius, and the thermal velocity of electron plays a dominant role in these regimes;<sup>3</sup> on the other hand for the cold electron case, the effects are important if the perpendicular wavelength is comparable to the electron inertial length and the Alfvén velocity dominates this regime.<sup>4</sup>

The existence of kinetic Alfvén waves has been established by satellite observation in various regions of Earth's magnetosphere, e.g., magnetopause,<sup>5,6</sup> auroral region,<sup>7-9</sup> plasma sheet boundary layer,<sup>10-14</sup> and central plasma sheet.<sup>15</sup> Recently, Van Allen Probe B observed broadband Alfvénic waves inside the plasmasphere driven by an impulsive solar wind pressure enhancement. These waves were modulated by

ULF oscillations and have been identified as Doppler-shifted kinetic Alfvén waves.<sup>16</sup> Magnetospheric Multiscale (MMS) observations revealed the presence of KAWs in the dayside magnetopause region.<sup>17</sup>

Various theoretical models based on different instabilities have been proposed to explain the observed ULF wave phenomena: for example, Kelvin-Helmholtz instability,<sup>18-21</sup> kinetic Alfvén waves,<sup>1,3,4,22-26</sup> and velocity shear driven instability.<sup>27,28</sup> These models were able to explain some of the observed characteristics of the KAWs. The localization and generation of turbulence in KAWs in various regions of Earth's magnetosphere have been studied through simulations.<sup>29-32</sup>

Lakhina<sup>27</sup> discussed the velocity shear as a possible source for the generation of these KAWs by considering a three component plasma model of which all the species, i.e., background ions, electrons, and beam ions, have a Maxwellian velocity distribution function. The study of Lakhina<sup>27</sup> was extended by Barik *et al.*<sup>28</sup> to examine the combined effect of ion beam and velocity shear in exciting the KAWs. They have shown that the ion beam and velocity shear acting as dual sources can excite the KAWs with larger growth rates and higher frequencies as compared to the case of velocity shear alone. These models considered the particle distributions as Maxwellian. In space plasmas, often

particle distributions depart from Maxwellian and have high energy tails. These distributions are known as nonthermal distribution, and one such distribution which is more commonly observed in various regions of Earth's magnetosphere is kappa-distribution.<sup>33-37</sup> Ogasawara *et al.*<sup>38</sup> have confirmed the existence of energetic electrons in the low altitude auroral ionosphere. Many theoretical studies have been carried out so far to explain the instabilities in Earth's magnetosphere due to the presence of nonthermal distribution. Summers and Thorne<sup>39</sup> have described the dispersion relation using the kappa distribution. Rubab *et al.*<sup>40-42</sup> have studied the KAW instability in Lorentzian dusty plasmas. Basu<sup>43</sup> has studied shear kinetic Alfvén waves in a homogeneous plasma having kappa particle distribution. In this work, we propose to study the KAWs driven by velocity shear in nonthermal plasma. A theoretical model includes the kappa electron along with Maxwellian ions and the beam ion having shear. The effect of kappa electrons on the excitation of KAWs is studied in detail. The layout of the paper is as follows: In Sec. II, a three component theoretical model of KAWs is presented. In Sec. III, the dispersion relation is derived followed by resonant instability analysis. The numerical results are delineated in Sec. IV. Finally, conclusions are drawn in Sec. V with an application of our model to the auroral region.

## II. THEORETICAL MODEL

We consider a three component plasma model for examining the resonant instability of Kinetic Alfvén Waves. The theoretical model includes background ions (protons,  $N_p$ ,  $T_i$ ) and beam ions ( $N_B$ ,  $T_B$ ), both having drifting Maxwellian distribution, and electrons ( $N_e$ ,  $T_e$ ) having kappa distribution. The quasineutrality condition is satisfied by the relation  $N_e = N_i + N_B$ . The plasma species are characterized by their temperature  $T_j$  and number density,  $N_j$ , where,  $j = i, e, B$  stand for background ions (protons), electrons, and beam ions, respectively. The general geometry of the model is as follows: the ambient magnetic field is directed in the  $z$ -direction; the propagation vector  $\mathbf{k}$  and the wave electric field are in the  $y$ - $z$  plane.

The nonthermal kappa distribution which can be used as the zeroth order distribution function for any plasma species is given by<sup>39</sup>

$$f_{0j}(v_{\perp}, v_{\parallel}) = \pi^{-3/2} \frac{1}{\theta_j^3} \frac{\Gamma(\kappa + 1)}{\kappa^{3/2} \Gamma(\kappa - 1/2)} \times N_j \left( 1 + \frac{v_{\perp}^2}{\kappa \theta_j^2} + \frac{(v_{\parallel} - V_j(X))^2}{\kappa \theta_j^2} \right)^{-(\kappa+1)} \quad (1)$$

Here,  $\Gamma$  represents the usual gamma function,  $\kappa$  is the nonthermal index that represents the nonthermal property of species, i.e., smaller the  $\kappa$  value, higher the nonthermality, and the parameter  $\theta_j$  is the modified thermal speed and related to usual thermal speed of species through the relation

$$\theta_j = \left[ \left( \frac{\kappa - 3/2}{\kappa} \right) \right]^{1/2} \alpha_j \quad (2)$$

Here,  $v_{\parallel}$  and  $v_{\perp} = \sqrt{v_x^2 + v_y^2}$  are the velocities in the parallel and perpendicular direction,  $\alpha_j = \left( \frac{2T_j}{m_j} \right)^{1/2}$  is thermal speed of  $j$ th species, and parallel and perpendicular are defined with respect to the ambient magnetic field. Further,  $V_j(X)$  represents the nonuniform streaming of particles along the ambient magnetic field ( $z$ -direction), whereas,

$X = x + v_y/\omega_{cj}$  indicates the gradient in velocity along the  $x$ -direction, i.e., perpendicular to ambient magnetic field. Here,  $\omega_{cj} = \frac{e_j B_0}{cm_j}$  is the cyclotron frequency of the  $j$ th species,  $e_j$  and  $m_j$  are charge and mass of  $j$ -th species, and  $c$  is the speed of light. Nonthermality index  $\kappa$  should be  $>3/2$  for the validity of physically meaningful thermal speed.

Since we are considering electrons as superthermal, the distribution function given by Eq. (1) will be used to derive the dispersion relation. On the other hand, for protons and ion beams, Maxwellian distribution function is obtained from Eq. (1) in the limit  $\kappa \rightarrow \infty$ . In the low plasma  $\beta$  (ratio of thermal pressure to magnetic pressure), it is better to write the electric field as the gradient of two different scalar potentials,<sup>44</sup> i.e., one along the parallel direction  $\psi$  and other along the perpendicular direction  $\phi$ ,

$$\mathbf{E} = -\nabla_{\perp} \phi + E_{\parallel} \hat{z}, \quad (3)$$

where  $E_{\parallel} = -\nabla_{\parallel} \psi$  is the parallel component of the wave electric field. The Poisson's equation takes the form

$$-\nabla_{\perp}^2 \phi + \frac{\partial E_{\parallel}}{\partial z} = 4\pi \sum_j e_j n_j. \quad (4)$$

The  $z$ -component of the Ampère's law is given by

$$\frac{\partial \nabla_{\perp}^2 \phi}{\partial z} + \nabla_{\perp}^2 E_{\parallel} = \frac{4\pi}{c^2} \frac{\partial}{\partial t} \sum_j J_{zj}. \quad (5)$$

It is worth mentioning that while deriving Eq. (5), the factor  $(\nabla_{\perp} \nabla_{\parallel} \mathbf{E}_{\parallel} - \nabla_{\parallel}^2 \mathbf{E}_{\perp})$  is neglected in comparison to  $(\nabla_{\parallel} \nabla_{\perp} \mathbf{E}_{\perp} - \nabla_{\perp}^2 \mathbf{E}_{\parallel})$  which means that the perpendicular component of current density  $J_{\perp}$  is neglected in comparison to  $J_z$  by assuming nearly perpendicular propagation of the waves, i.e.,  $k_{\perp} \gg k_{\parallel}$ .

Here, the number density  $n_j$  and  $z$ -component of the current density  $J_{zj}$  of the  $j$ th species are given by expressions

$$n_j = \int d^3 v f_{1j}, \quad J_{zj} = \int d^3 v e_j v_z f_{1j}, \quad (6)$$

where the perturbed distribution function  $f_{1j}$  can be derived from the linearized Vlasov's equation by following the standard procedures of Swanson [*Plasma Waves* by D. G. Swanson, 2nd ed., Eq. (4.169)].<sup>45</sup> For this, the perturbation is assumed to be of the form  $f_{1j} = \exp(ik_{\perp} y + ik_{\parallel} z - i\omega t)$ , where  $\omega$  is the frequency of the wave, and  $k_{\perp}$  and  $k_{\parallel}$  are the perpendicular and parallel components of wave propagation vector  $\mathbf{k}$  respectively. Further, we use a local approximation ( $L_j k \gg 1$ ) to solve the linearized Vlasov's equation, where  $L_j = V_j \left( \frac{dv_j}{dx} \right)^{-1}$  is the velocity gradient scale length and  $k$  is the wave number. The perturbed distribution is obtained by performing integrations over unperturbed orbits and is given by the expression<sup>27,28</sup>

$$f_{1j} = \frac{e_j}{m_j} \sum_{n=-\infty}^{+\infty} \sum_{m=-\infty}^{+\infty} \frac{e^{i(n-m)\theta}}{(k_{\parallel} v_z - \omega + n\omega_{cj})} J_n(\xi_j) J_m(\zeta_j) \times (k_{\perp} M_j \phi + k_{\parallel} L_j \psi), \quad (7)$$

where coefficients  $M_j$  and  $L_j$  can be expressed as<sup>27,28</sup>

$$M_j = \left(1 - \frac{k_{\parallel} v_z}{\omega}\right) \left[ \frac{\partial f_{0j}}{\partial v_{\perp}} \cdot \frac{n\omega_{cj}}{k_{\perp} v_{\perp}} + \frac{1}{\omega_{cj}} \cdot \frac{\partial f_{0j}}{\partial x} \right] + \frac{\partial f_{0j}}{\partial v_z} \frac{n\omega_{cj} k_{\parallel}}{k_{\perp} \omega}, \quad (8)$$

$$L_j = \frac{k_{\perp} v_z}{\omega} \left[ \frac{\partial f_{0j}}{\partial v_{\perp}} \cdot \frac{n\omega_{cj}}{k_{\perp} v_{\perp}} + \frac{1}{\omega_{cj}} \cdot \frac{\partial f_{0j}}{\partial x} \right] + \left(1 - \frac{n\omega_{cj}}{\omega}\right) \frac{\partial f_{0j}}{\partial v_z}. \quad (9)$$

Here,  $J_n(\xi_j)$  and  $J_m(\xi_j)$  are the Bessel function of order  $n$  and  $m$ , respectively, with arguments  $\xi_j = \frac{k_{\perp} v_{\perp}}{\omega_j}$ ; the term  $\left(\frac{1}{\omega_j} \cdot \frac{\partial f_{0j}}{\partial x}\right)$  comes from the contribution of velocity shear. In Eqs. (8) and (9),  $f_{0j}$  represents the zeroth order distribution function. Using zeroth order Maxwellian and kappa distribution functions in Eq. (7), the corresponding perturbed distribution function  $f_{1j}$  is obtained. Subsequently, the perturbed number density  $n_j$  and the  $z$ -component of current density  $J_{zj}$  are obtained for the electrons, ions, and ion beam from Eq. (6). For Maxwellian distribution function, these

are given by Eqs. (10) and (11) of Barik *et al.*<sup>28</sup> and can be used for ions and ion beam in our model. The perturbed number ( $n_j$ ) and current ( $J_{zj}$ ) densities for electrons which follow the  $\kappa$  distribution are given by

$$n_e = - \sum_{n=-\infty}^{+\infty} \frac{4eN_e}{m_e \theta_e^2} \left(\frac{\omega_{ce}}{k_{\perp} \theta_e}\right)^2 \left\{ \left(\frac{n\omega_{ce}}{\omega}\right) \times \left[ \left\{ \frac{n\omega_{ce}}{k_{\parallel} \theta_e} - (d-1)\eta_{ne^-} \right\} F - dG \right] \phi + \left[ \left\{ \frac{n\omega_{ce}}{\omega} \chi_n - (d+1) \frac{\chi_n}{\chi_0} \eta_{ne^-} \right\} F + \left\{ \frac{n\omega_{ce}}{\omega} - \frac{\chi_n}{\chi_0} (d-1) \right\} G \right] \psi \right\}. \quad (10)$$

The parallel current density of the electron is given by

$$J_{ze} = - \sum_{n=-\infty}^{+\infty} \frac{2e^2 N_e}{m_e \theta_e} \left(\frac{\omega_{ce}}{k_{\perp} \theta_e}\right)^2 \times \left\{ \left[ \left\{ \frac{2n\omega_{ce}}{\omega} \chi_n \eta_{0e^-} - 2d \frac{\chi_n}{\chi_0} [\chi_n^2 + \eta_{ne^-} \eta_{0e^+}] + 2d \frac{V_e^2(X)}{\theta_e^2} \left[ \frac{(2\eta_{ne^-} - 1)}{\chi_0} \right] \right\} F + \left\{ \frac{2n\omega_{ce}}{\omega} \eta_{0e^-} - 2d \left[ \frac{\chi_n}{\chi_0} \left( \eta_{0e^+} + \frac{V_e(X)}{\theta_e} \right) + \frac{\eta_{ne^-} \eta_{ne^+}}{\chi_0} \right] \right\} G - \frac{d}{\chi_0} H \right] \phi + \left[ \left\{ 2\chi_n^2 \left[ \frac{n\omega_{ce}}{\omega} - (d-1) \frac{\eta_{ne^-}}{\chi_0} \right] + 6d \frac{V_e^2(X)}{\theta_e^2} \frac{\eta_{ne^-}}{\chi_0} \right\} F + \left\{ \frac{2n\omega_{ce}}{\omega} \eta_{ne^+} - 2 \frac{\chi_n^2}{\chi_0} (d-1) + 6 \frac{d}{\chi_0} \frac{V_e^2(X)}{\theta_e^2} \right\} G - \frac{d}{\chi_0} H \right] \psi \right\}, \quad (11)$$

where

$$F = \left\{ \frac{1}{2^{|n|}} \frac{\kappa^{|n|} \Gamma(\kappa - |n| - 1/2)}{\Gamma(|n| + 1) \Gamma(\kappa - 1/2)} \left(\frac{\kappa - |n|}{\kappa}\right)^{3/2} \lambda_e^{|n|+1} Z_{\kappa-|n|}^* \times \left[ \left(\frac{\kappa - |n|}{\kappa}\right)^{1/2} \eta_{ne} + \dots \right] \right\}, \quad (12)$$

$$G = \left\{ \frac{1}{2^{|n|}} \frac{\kappa^{|n|-1} \Gamma(\kappa - |n| + 1/2)}{\Gamma(|n| + 1) \Gamma(\kappa - 1/2)} \lambda_e^{|n|+1} + \dots \right\}, \quad (13)$$

$$H = \left\{ \frac{1}{2^{|n|}} \frac{\kappa^{|n|} \Gamma(\kappa - |n| - 1/2)}{\Gamma(|n| + 1) \Gamma(\kappa - 1/2)} \lambda_e^{|n|+1} + \dots \right\}. \quad (14)$$

Here, the  $F$  and  $H$  associated terms are valid for the condition  $\kappa > |n| + 1/2$ , whereas the  $G$  associated terms are valid for  $\kappa > |n| - 1/2$ .

Here,  $\lambda_e = \frac{1}{2} \frac{k_{\perp}^2 \theta_e^2}{\omega_{ce}^2}$ ,  $\theta_e = \left[ \left(\frac{\kappa - 3/2}{\kappa}\right)^{1/2} \frac{(2T_e)}{m_e} \right]^{1/2}$  and  $S_e = \frac{1}{\omega_{ce}} \cdot \left(\frac{dV_e(X)}{dx}\right)$  are the modified thermal speed and velocity shear of electrons, respectively,  $\eta_{ne^{\pm}} = \frac{\omega - n\omega_{ce} \pm k_{\parallel} V_e(X)}{k_{\parallel} \theta_e}$ ,  $\eta_{0e^{\pm}} = \frac{\omega \pm k_{\parallel} V_e(X)}{k_{\parallel} \theta_e}$ ,  $d = S_e \frac{k_{\perp}}{k_{\parallel}}$ ,  $\chi_n = \frac{(\omega - n\omega_{ce})}{k_{\parallel} \theta_e}$ ,  $\chi_0 = \frac{\omega}{k_{\parallel} \theta_e}$  and  $Z_{\kappa+1}^*$  is the modified plasma dispersion function (MPDF) given by<sup>39,46</sup>

$$Z_{\kappa}^*(\xi_j) = \frac{1}{\sqrt{\pi} \kappa^{3/2} \Gamma(\kappa - 1/2)} \int_{-\infty}^{\infty} \frac{ds}{(s - \xi)(1 + s^2/\kappa)^{\kappa+1}}; \quad (15)$$

$$Im(\xi_j) > 0,$$

where “ $s$ ” is any arbitrary variable. Equation (15) represents the modified plasma dispersion function of order  $\kappa$ . The MPDF of any desired order can be obtained by replacing  $\kappa$  with the respective order in Eq. (15). The number and current densities given by Eqs. (10) and (11) for electrons have been obtained in the limit  $\lambda_e \rightarrow 0$ ; however, they can be used in the same limit for any other species having kappa distribution. By assuming that an electron has no drift velocity, i.e.,  $V_e = 0$  and shear flow, i.e.,  $S_e = 0$ , Eqs. (10) and (11) are reduced to

$$n_e = - \sum_{n=-\infty}^{+\infty} \frac{4eN_e}{m_e \theta_e^2} \left(\frac{\omega_{ce}}{k_{\perp} \theta_e}\right)^2 \left\{ \left[ \left(\frac{n\omega_{ce}}{k_{\parallel} \theta_e}\right) F \right] \phi + \left[ \chi_n \left(\frac{2n\omega_{ce}}{\omega} - 1\right) F + G \right] \psi \right\}, \quad (16)$$

$$J_{ze} = - \sum_{n=-\infty}^{+\infty} \frac{2e^2 N_e}{m_e \theta_e} \left(\frac{\omega_{ce}}{k_{\perp} \theta_e}\right)^2 \left[ (\chi_n F + G) \left(\frac{2n\omega_{ce}}{k_{\parallel} \theta_e} \phi + 2\chi_n \psi\right) \right]. \quad (17)$$

Thereafter, substituting the values of perturbed number densities,  $n_j$  and current densities  $J_{zj}$  (i.e., for all the three species, ions, electrons, and beam ions) in Eqs. (4) and (5) and simplifying, we obtain following equations:

$$D_{11}\phi + D_{12}\psi = 0, \tag{18}$$

$$D_{21}\phi + D_{22}\psi = 0, \tag{19}$$

where the coefficients are given by the expressions

$$D_{11} = k_{\perp}^2 \left[ 1 + \left( \frac{\kappa - 1}{\kappa} \right)^{1/2} \left\{ \frac{\omega_{pe}^2}{\omega_{ce}^2} \right\} + \sum_l \frac{2\omega_{pl}^2 \bar{\omega}}{k_{\perp}^2 \alpha_l^2 \omega} (1 - b_l) \right], \tag{20}$$

$$D_{12} = k_{\perp}^2 \left[ 1 + \frac{\omega_{pe}^2}{k_{\perp}^2 \theta_e^2} \left\{ \frac{(2\kappa - 1)}{\kappa} + \frac{i\sqrt{\pi}\kappa!}{\kappa^{3/2}\Gamma(\kappa - 1/2)} \left( \frac{2\omega}{k_{\parallel}\theta_e} \right) \right\} - \sum_l \frac{\omega_{pl}^2 b_l}{k_{\perp}^2 \alpha_l^2} Z' \left( \frac{\bar{\omega}}{k_{\parallel}\alpha_l} \right) \left( 1 - S_l \frac{k_{\perp}}{k_{\parallel}} \right) \right], \tag{21}$$

$$D_{21} = k_{\parallel} k_{\perp}^2 \left[ 1 + \sum_l \frac{\omega_{pl}^2 b_l}{c^2 k_{\perp}^2} S_l \frac{k_{\perp}}{k_{\parallel}} \right], \tag{22}$$

$$D_{22} = -k_{\parallel} k_{\perp}^2 \left[ 1 - \frac{\omega_{pe}^2}{c^2 k_{\perp}^2} \left\{ \frac{(2\kappa - 1)}{\kappa} \frac{\omega^2}{k_{\parallel}^2 \theta_e^2} + \frac{i\sqrt{\pi}\kappa!}{\kappa^{3/2}\Gamma(\kappa - 1/2)} \frac{2\omega^3}{k_{\parallel}^3 \theta_e^3} \right\} + \sum_l \frac{\omega_{pl}^2}{c^2 k_{\perp}^2} \left\{ \frac{b_l \omega^2}{k_{\parallel}^2 \alpha_l^2} Z' \left( \frac{\bar{\omega}}{k_{\parallel}\alpha_l} \right) \left( 1 - S_l \frac{k_{\perp}}{k_{\parallel}} \right) + S_l \frac{k_{\perp}}{k_{\parallel}} \right\} \right]. \tag{23}$$

Please note that we have separated out electron contribution in Eqs. (20)–(23) and summation is only for ions and ion beam. Thus, we define  $\omega_{pe} = \left( \frac{4\pi N_e e^2}{m_e} \right)^{1/2}$ , which is the plasma frequency of electrons,  $\omega_{pl} = \left( \frac{4\pi N_l e^2}{m_l} \right)^{1/2}$ , which is the plasma frequency of  $l$ th species, where  $l$  stands for  $i$  and  $B$  for background ions and beam ions, respectively,  $\bar{\omega} = \omega - k_{\parallel} V_l$  is the Doppler shifted frequency of  $l$ th species,  $S_l$  is the velocity shear, and  $\alpha_l = \left( \frac{2T_l}{m_l} \right)^{1/2}$  is the thermal speed of  $l$ th species, respectively.

### III. DISPERSION RELATION

In this section, a dispersion relation is derived for KAWs in the three-component model of Maxwellian ions, ion beam with velocity shear, and superthermal electrons. We proceed in a similar fashion as Lakhina<sup>27</sup> and Barik *et al.*<sup>28</sup> by assuming shear in the ion beam only, i.e.,  $S = S_B$  and  $V_i = 0 = V_e$ . Further, we make the following assumptions: cold background ions,  $\omega^2 \gg k_{\parallel}^2 \alpha_i^2$ , hot electrons,  $\omega \ll k_{\parallel} \alpha_e$ ,  $\lambda_e \ll 1$ , and hot ion beam,  $\bar{\omega} \leq k_{\parallel} \alpha_B$  which acts as a free energy source. Using the above listed assumptions, the following dispersion relation is obtained by equating the determinant of the coefficients of  $\phi$  and  $\psi$  to zero in Eqs. (18) and (19):

$$\begin{aligned} & \frac{b_i N_i}{N_e} \left[ 1 + a_1 - \frac{\omega^2}{k_{\parallel}^2 V_A^2} \frac{N_i}{N_e} \frac{1 - b_i}{\lambda_i} A q_0 \right] \\ & - \frac{\omega^2}{k_{\parallel}^2 c_s^2} \left[ C'_R + i(1 + a_1) C_I - \frac{\omega^2}{k_{\parallel}^2 V_A^2} \frac{N_i}{N_e} \frac{1 - b_i}{\lambda_i} A (C_R + i C_I) \right] \\ & = \frac{2\omega^2 (1 - b_i) N_i}{k_{\parallel}^2 \alpha_i^2 N_e}, \end{aligned} \tag{24}$$

where

$$a_1 = \frac{N_B \beta_B b_B}{N_e} S \frac{k_{\perp}}{k_{\parallel}}, \tag{25}$$

$$q_0 = 1 + \frac{N_B m_i}{N_i m_B} \frac{S k_{\perp}}{b_i k_{\parallel}}, \tag{26}$$

$$A = 1 + \frac{N_B T_i \bar{\omega} (1 - b_B)}{N_i T_B \omega (1 - b_i)}, \tag{27}$$

$$C_R = \frac{(2\kappa - 1)}{(2\kappa - 3)} + \frac{N_B T_e}{N_e T_B} b_B \left( 1 - S \frac{k_{\perp}}{k_{\parallel}} \right), \tag{28}$$

$$C'_R = \frac{(2\kappa - 1)}{(2\kappa - 3)} + \frac{N_B T_e}{N_e T_B} \left\{ b_B \left( 1 - \frac{\bar{\omega}}{\omega} \right) + \left( \frac{\bar{\omega}}{\omega} - b_B S \frac{k_{\perp}}{k_{\parallel}} \right) \right\} + a_1 C_R, \tag{29}$$

$$\begin{aligned} C_I &= \sqrt{\pi} \frac{\omega}{k_{\parallel} \theta_e} \left[ \frac{\kappa!}{\kappa^{3/2} \Gamma(\kappa - 1/2)} \frac{2\kappa}{(2\kappa - 3)} \right. \\ & \quad \left. + b_B \frac{N_B}{N_e} \left( \frac{T_e}{T_B} \right)^{3/2} \left( \frac{m_B}{m_e} \right)^{1/2} \frac{\bar{\omega}}{\omega} \left( 1 - S \frac{k_{\perp}}{k_{\parallel}} \right) \right. \\ & \quad \left. \times \left( \frac{2\kappa - 3}{2\kappa} \right)^{1/2} \exp \left( - \frac{\bar{\omega}^2}{k_{\parallel}^2 \alpha_B^2} \right) \right]. \end{aligned} \tag{30}$$

In the above expressions, the coefficients  $a_1$ ,  $q_0$ , and  $A$  are the same as obtained by Lakhina<sup>27</sup> and Barik *et al.*,<sup>28</sup> whereas the coefficients  $C_R$ ,  $C'_R$ , and  $C_I$  differ from their expressions by factors involving  $\kappa$ . These factors arise due to the presence of the kappa electron in our model in place of the Maxwellian electron considered in their model. In the limit of  $\kappa \rightarrow \infty$ , these expressions will become exactly the same as in Lakhina<sup>27</sup> and Barik *et al.*<sup>28</sup> Here,  $V_A = (B_0^2/4\pi N_e m_i)^{1/2}$  is the Alfvén speed,  $c_s = (T_e/m_i)^{1/2}$  is the ion acoustic speed,  $b_l = I_0(\lambda_l) \exp(-\lambda_l)$ ,  $I_0(\lambda_l)$  is the zeroth order modified Bessel function with argument  $\lambda_l = k_{\perp}^2 \rho_l^2 (\rho_l^2 = \alpha_l^2/2\omega_{cl}^2)$ , where  $l = i$  and  $B$  for ions and beam ions, respectively,  $\beta_i = (4\pi N_e T_i/B_0^2)$  and  $\beta_B = (4\pi N_e T_B/B_0^2)$  are the ion and beam plasma betas, respectively, and  $C_I$  represents the damping term due to electrons and beam ions.

In the absence of ion beam ( $N_B = 0$ ) and electron damping, the dispersion relation Eq. (24) will reduce to following:

$$\left[ b_i - \frac{(2\kappa - 1)}{(2\kappa - 3)} \frac{\omega^2}{k_{\parallel}^2 c_s^2} \right] \cdot \left[ 1 - \frac{\omega^2}{k_{\parallel}^2 V_A^2} \frac{1 - b_i}{\lambda_i} \right] = \frac{2\omega^2 (1 - b_i)}{k_{\parallel}^2 \alpha_i^2}, \tag{31}$$

which shows coupling between two normal modes, i.e., kinetic Alfvén wave and the ion acoustic wave in the presence of  $\kappa$  distribution. In the limit  $\kappa \rightarrow \infty$ , Eq. (31) reduces to the coupling equation described by Hasegawa and Chen<sup>3</sup> [cf. Eq. (36)] and Lakhina<sup>27</sup> [cf. Eq. (23)].

In the low plasma  $\beta$  limit, i.e.,  $\beta \ll 1$ , coupling between the two modes becomes weak, and they decouple giving rise to the dispersion relation of kinetic Alfvén wave as

$$\omega^2 \approx k_{\parallel}^2 V_A^2 \left[ \frac{\lambda_i}{(1 - b_i)} + \frac{(2\kappa - 3) T_e}{(2\kappa - 1) T_i} \lambda_i \right] \tag{32}$$

and for the ion acoustic wave as

$$\omega^2 \approx b_i k_{\parallel}^2 c_s^2 \left[ \frac{(2\kappa - 1)}{(2\kappa - 3)} + \frac{T_e (1 - b_i)}{T_i} \right]^{-1}. \tag{33}$$

Further, in the limit  $\kappa \rightarrow \infty$ , Eqs. (32) and (33) reduce to Eqs. (24) and (25) of Lakhina,<sup>27</sup> respectively. In the limit  $\lambda_i \ll 1$ , dispersion Eq. (32) can be further simplified to

$$\omega^2 \approx k_{\parallel}^2 V_A^2 \left[ 1 + k_{\perp}^2 \rho_i^2 \left\{ \frac{3}{4} + \frac{(2\kappa - 3) T_e}{(2\kappa - 1) T_i} \right\} \right]. \quad (34)$$

Equation (34) is the same as Eq. (8) of Khan *et al.*<sup>47</sup> Here  $\rho_i = (\alpha_i / \sqrt{2\omega_{ci}})$  is the ion gyroradius.

It is clearly noticeable that Eq. (24) contains real as well as the imaginary terms, so we can write the dispersion relation as a combination of real and imaginary parts

$$D_R(\omega, \mathbf{k}) + iD_I(\omega, \mathbf{k}) = 0, \quad (35)$$

where

$$D_R(\omega, k) = \frac{\omega^4}{k_{\parallel}^4 V_A^4} \left[ \frac{N_i (1 - b_i)}{N_e} \frac{A C_R}{\lambda_i} \right] - g \frac{\omega^2}{k_{\parallel}^2 V_A^2} + \frac{N_i b_i \beta_i T_e}{N_e} \frac{1 + a_1}{2 T_i}, \quad (36)$$

$$D_I(\omega, k) = -\frac{\omega^2}{k_{\parallel}^2 V_A^2} \left[ 1 + a_1 - \frac{\omega^2 (1 - b_i) N_i}{k_{\parallel}^2 V_A^2} \frac{N_i}{N_e} A \right] C_I, \quad (37)$$

$$g = \left[ C'_R + \frac{N_i}{N_e} (1 - b_i) \frac{T_e}{T_i} \left\{ 1 + \frac{N_i b_i \beta_i}{N_e} A q_0 \right\} \right]. \quad (38)$$

### A. Resonant instability

The resonant instability of the system occurs when the thermal speed of the beam ions is comparable with the parallel phase velocity of the wave, i.e.,  $\bar{\omega} \leq k_{\parallel} \alpha_B$ . Assuming  $\omega = \omega_r + i\gamma$ , where  $\omega_r$  is the real frequency and  $\gamma \ll \omega_r$ , the growth/damping of the wave  $\gamma$  can be given by the expression

$$\gamma = -\frac{D_I(\omega_r, \mathbf{k})}{\partial D_R(\omega_r, \mathbf{k}) / \partial \omega_r}, \quad (39)$$

where  $D_R$  and  $D_I$  are given by Eqs. (36) and (37), respectively, and contain terms corresponding to ion beam velocity as well as velocity shear. In this section, we study the role of the velocity shear alone in the excitation of KAWs. Thus, under the assumption of low ion beam velocity, i.e.,  $k_{\parallel} V_B \ll \omega$ , in Eqs. (36) and (37), the contribution of ion beam velocity vanishes, and the only source of free energy to drive the instabilities is velocity shear. Therefore, now the resonant condition would be  $\omega \leq k_{\parallel} \alpha_B$  for the above-mentioned case. The real frequency is obtained by solving  $D_R(\omega, \mathbf{k}) = 0$  and is given by the following expression

$$\omega^2 = \frac{k_{\parallel}^2 V_A^2}{2} \frac{\lambda_i N_e}{(1 - b_i) A_1 N_i C_R} \left[ g_1 \pm (g_1^2 - 4g_0)^{1/2} \right], \quad (40)$$

and the growth rate/damping is given by

$$\gamma = \frac{\omega_r}{2(g_1^2 - 4g_0)^{1/2}} \left[ 1 + a_1 - \frac{\omega_r^2 (1 - b_i) N_i}{k_{\parallel}^2 V_A^2} \frac{N_i}{N_e} A_1 \right] C_{I1}, \quad (41)$$

where the various coefficients are

$$A_1 = 1 + \frac{N_B T_i (1 - b_B)}{N_i T_B (1 - b_i)}, \quad (42)$$

$$g_0 = \left( \frac{N_i}{N_e} \right)^2 \frac{b_i \beta_i T_e (1 - b_i)}{2 T_i \lambda_i} (1 + a_1) A_1 C_R, \quad (43)$$

$$g_1 = \left[ C'_{R1} + \frac{N_i}{N_e} (1 - b_i) \frac{T_e}{T_i} \left\{ 1 + \frac{N_i b_i \beta_i}{N_e} \frac{A_1 q_0}{2 \lambda_i} \right\} \right], \quad (44)$$

$$C'_{R1} = \frac{(2\kappa - 1)}{(2\kappa - 3)} + \frac{N_B T_e}{N_e T_B} \left( 1 - b_B S \frac{k_{\perp}}{k_{\parallel}} \right) + a_1 C_R, \quad (45)$$

$$C_{I1} = \sqrt{\pi} \frac{\omega}{k_{\parallel} \theta_e} \left[ \frac{\kappa!}{\kappa^{3/2} \Gamma(\kappa - 1/2)} \frac{2\kappa}{(2\kappa - 3)} + b_B \frac{N_B}{N_e} \left( \frac{T_e}{T_B} \right)^{3/2} \left( \frac{m_B}{m_e} \right)^{1/2} \left( 1 - S \frac{k_{\perp}}{k_{\parallel}} \right) \times \left( \frac{2\kappa - 3}{2\kappa} \right)^{1/2} \exp \left( -\frac{\omega^2}{k_{\parallel}^2 \alpha_B^2} \right) \right]. \quad (46)$$

### IV. NUMERICAL ANALYSIS

The normalized real frequency obtained from Eq. (40) and the growth rate from Eq. (41) are plotted with the square of the normalized perpendicular wave number  $\lambda_B = \frac{k_{\perp}^2 \alpha_B^2}{2\omega_{cB}^2}$ . For the numerical analysis purposes, all the parameters are normalized in the similar way as mentioned in the work of Barik *et al.*,<sup>28</sup> i.e., frequencies are normalized with respect to the cyclotron frequency of the beam ion,  $\omega_{cB}$ , temperatures with beam ion temperature,  $T_B$ , streaming velocity,  $V_B$ , with thermal speed of beam ion,  $\alpha_B$ , and the normalized velocity shear  $S = \frac{1}{\omega_{cB}} \cdot \left( \frac{dV_B(X)}{dx} \right)$ . From the numerical calculation, it is found that for the growth of the KAWs,  $C_R > 0$  and  $C_I < 0$ . The condition  $C_R > 0$  puts an upper limit on the value of the velocity shear given by

$$S_{max} = \frac{k_{\parallel}}{k_{\perp}} \left[ 1 + \frac{(2\kappa - 1) N_e T_B}{(2\kappa - 3) N_B b_B T_e} \right]. \quad (47)$$

Figure 1 shows the variation of maximum velocity shear with the nonthermal index  $\kappa$  which is obtained from Eq. (47) for various parameters listed on the respective curves. In each panel, the black curve represents the variation of velocity shear with  $\kappa$  for the plasma parameters  $\frac{N_B}{N_e} = 0.5$ ,  $\frac{k_{\parallel}}{k_{\perp}} = 0.01$  and  $T_B/T_e = 5.0$ , whereas the red curve shows the variation of the respective parameters mentioned on the curves. For each variation, other parameters are kept fixed. Figure 1(a) shows the variation of velocity shear with  $\kappa$  for different ion beam densities. It is obvious from the graph that a very high velocity shear is required to excite the KAWs for  $\kappa$ - electrons in comparison to Maxwellian electrons. It is observed that larger velocity shear is required to excite the waves with a decrease in the ion number density for a fixed value of  $\kappa$ . This should happen because the increase in the number density of ion beam provides the extra energy required to compensate the absence of shear. In Fig. 1(b), the variation of velocity shear with  $\kappa$  is shown for different values of  $k_{\parallel}/k_{\perp}$  keeping all other parameters fixed as earlier. For a fixed value of  $\kappa$ , the velocity shear required to excite the waves decreases with the increase in the angle of propagation. Figure 1(c) shows the variation of velocity shear for different values of ion beam temperature. It is seen that velocity shear increases with the increase in  $T_B/T_e$  values for a fixed value of  $\kappa$ .

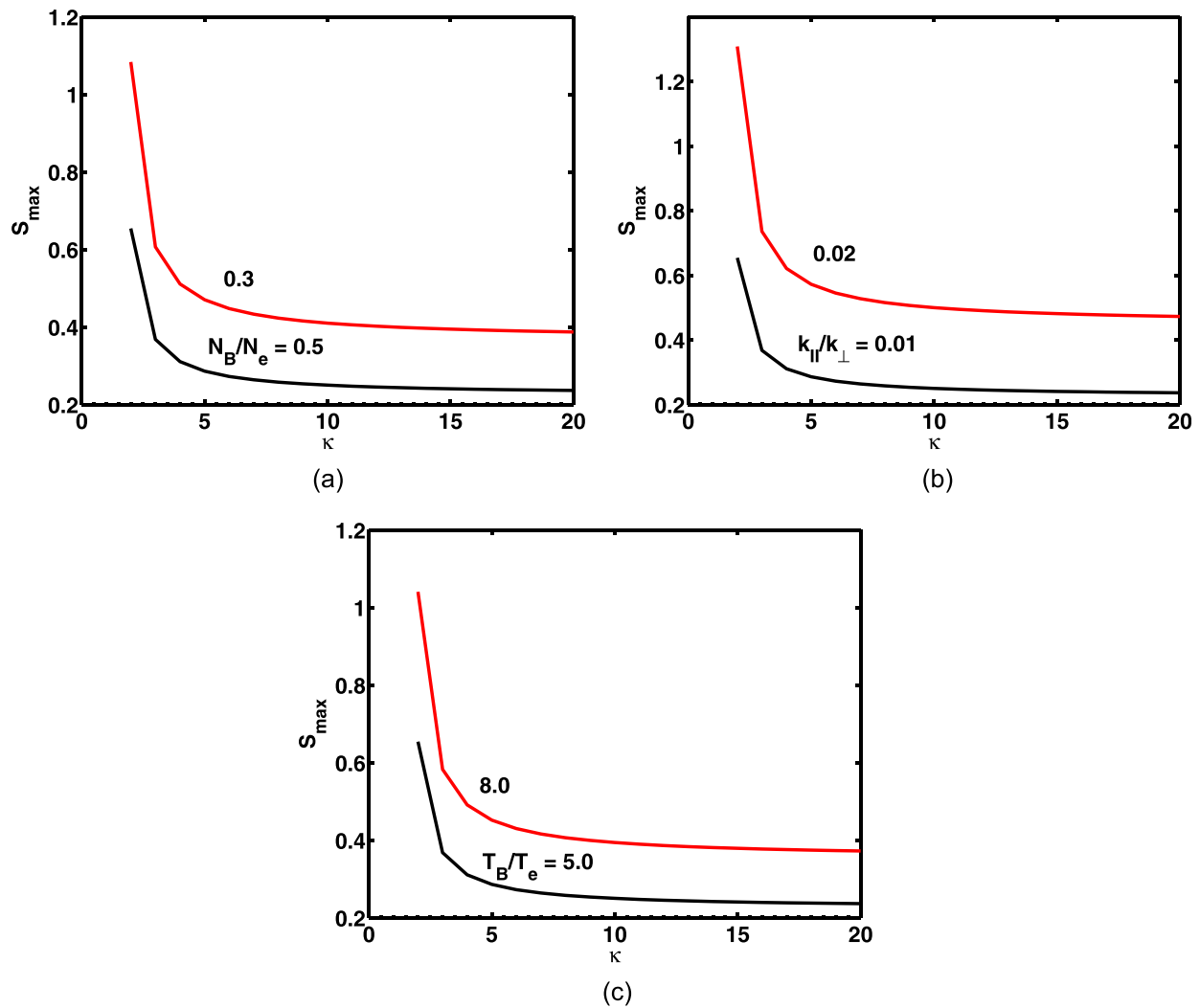


FIG. 1. KAWs Resonant instability driven by velocity shear: variation of velocity shear with the nonthermal index  $\kappa$  for (a)  $\frac{k_{\parallel}}{k_{\perp}} = 0.01$ ,  $T_B/T_e = 5.0$  and  $\frac{N_B}{N_e} = 0.5, 0.3$ , (b)  $\frac{N_B}{N_e} = 0.5$ ,  $T_B/T_e = 5.0$  and  $\frac{k_{\parallel}}{k_{\perp}} = 0.01, 0.02$ , and (c)  $\frac{N_B}{N_e} = 0.5$ ,  $\frac{k_{\parallel}}{k_{\perp}} = 0.01$  and  $\frac{T_B}{T_e} = 5.0, 8.0$ .

Thus, for relatively cold nonthermal electrons, more velocity shear is required to excite the waves. This could be due to the damping caused by the colder electrons.

Figures 2(a) and 2(b) show the variation of normalized real frequency and the growth rate with respect to the square of the normalized perpendicular wave number ( $\lambda_B$ ) for the fixed plasma parameters,  $N_B/N_e = 0.5$ ,  $\beta_i = 0.001$ ,  $k_{\parallel}/k_{\perp} = 0.01$ ,  $S = 0.3$ ,  $T_i/T_B = 0.016$ ,  $T_e/T_B = 0.2$ , and for various values of  $\kappa$  as mentioned on the curves. The above-mentioned parameters are common in all subsequent figures, except otherwise stated. It can be seen from Fig. 2 that with the decrease in  $\kappa$  values, i.e., tending toward more nonthermal electrons, the real frequency as well as the growth rate decreases and wave number range also narrows down. When the electron approaches Maxwellian distribution, the wave unstable region shifts toward higher wave numbers. It is noted that for a fixed value of  $\kappa$ , the

highest wave frequency corresponds to the lowest growth rate. Hence, from this, it is concluded that the kappa-electrons tend to suppress the growth rate of the KAWs.

Figures 3(a) and 3(b) represent the variation of normalized real frequency and growth rate with respect to  $\lambda_B$  at fixed  $\kappa = 3$  and  $\kappa = \infty$  for various values of velocity shear  $S$  as mentioned on the curves. At a fixed  $\kappa$ , when the velocity shear  $S$  increases, there is a marginal increase in real frequency, whereas the growth rate increases significantly. For Maxwellian electrons ( $\kappa = \infty$ ), it can be seen that for a fixed value of shear ( $S = 0.3$  here) both the real frequency and growth rate are maximum as compared to nonthermal electrons ( $\kappa = 3$ ). Although not shown here, it is observed that for a smaller value of  $\kappa$ , a larger shear is required for a significant growth of the waves. Numerical computations reveal that for  $\kappa = 2, 3$ , and  $4$ , threshold values of the shear are  $S \sim 0.048, 0.025$ , and  $\sim 0.021$ , respectively, to

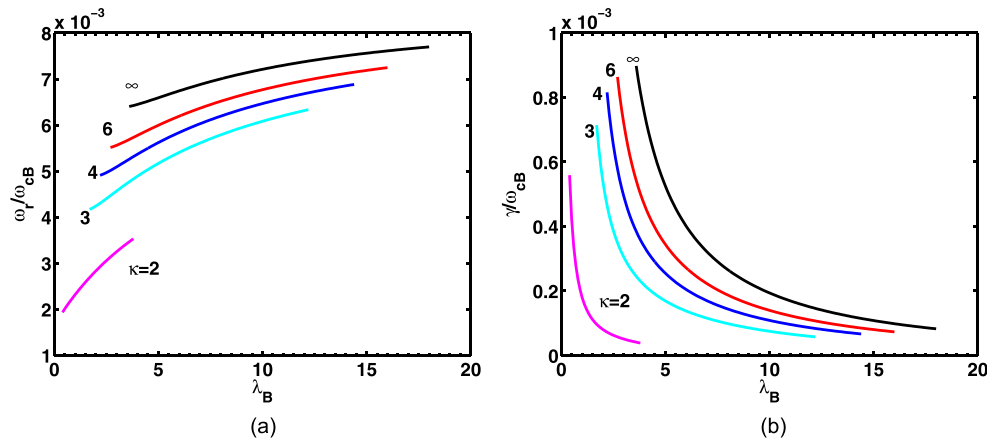


**FIG. 2.** KAW resonant instability driven by velocity shear: variation of (a) normalized real frequency,  $\omega_r/\omega_{cB}$ , and (b) normalized growth rate,  $\gamma/\omega_{cB}$  vs  $\lambda_B = \frac{k_{\perp}^2 v_B^2}{2\omega_{cB}^2}$  for  $N_B/N_e = 0.5$ ,  $\beta_i = 0.001$ ,  $\frac{k_{\parallel}}{k_{\perp}} = 0.01$ ,  $S = 0.3$  and various values of  $\kappa$  as listed on the curves.

excite the waves, whereas, for Maxwellian electrons, a threshold value of  $S = 0.017$  is required. These results are in accordance with Eq. (47). These results may have implications with the observation of Wygant *et al.*<sup>10</sup> during the substorm expansion phase. In the expansion phase of the substorm, the compression of Earth’s magnetosphere causes enhancement of velocity shear which produces increased growth rate of KAWs, thereby leading to enhanced Poynting flux of kinetic Alfvén waves toward the Earth.

The variation of normalized real frequency and growth rate with the velocity shear  $S$  for Maxwellian as well as  $\kappa$  electrons is depicted in Fig. 4 for  $\lambda_B (= 0.5)$ ,  $N_B/N_e = 0.3$ , and other fixed parameters are same as in Fig. 3. It is seen from Fig. 4 that the real frequency and growth rate increase with the increase in velocity shear as well as the decrease in nonthermality (increase in  $\kappa$ ). The highest growth rate is achieved for Maxwellian electrons for a fixed value of shear. Further, for the  $\kappa = 2$  curve, it can be seen that a very high velocity shear is required to reach the same level of growth as that of the  $\kappa = \infty$  curve. Hence, it

can be inferred that a nonthermal electron restricts the growth, whereas a Maxwellian electron facilitates the growth of the KAWs.

Figure 5 shows the variation of the normalized real frequency and growth rate with  $\lambda_B$  for various values of number density as mentioned on the curves for nonthermal ( $\kappa = 3$ ) and Maxwellian electrons ( $\kappa = \infty$ ). The growth rate increases with the increase in the ion beam density. However, it is observed that with the increase in number density, the real frequency and wave number range for which these waves are excited first increase for  $N_B/N_e \leq 0.31$  and then start to decrease for the higher values of  $N_B/N_e$ . Further, the real frequency as well as growth rate is higher for Maxwellian electrons ( $\kappa = \infty$ ) than the  $\kappa$  electrons, and waves are also excited for a larger  $\lambda_B$  range. Numerical computations reveal that the critical value of number density increases with the decrease in the nonthermal index  $\kappa$ , i.e., for highly nonthermal electrons (smaller  $\kappa$ ), a larger ion beam density  $N_B/N_e$  is required to excite the waves compared to the case of Maxwellian electrons. The critical values of number density are  $N_B/N_e = 0.07$  ( $\kappa = 2$ ),

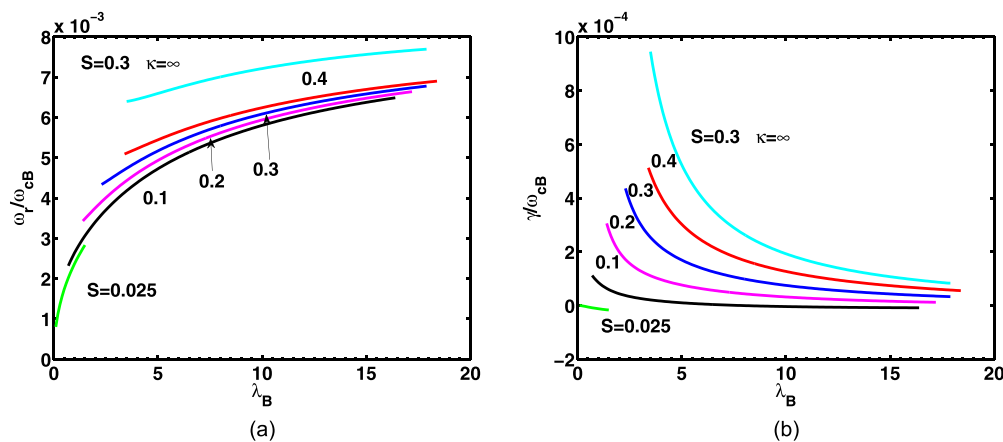


**FIG. 3.** KAW resonant instability driven by velocity shear: variation of (a) normalized real frequency,  $\omega_r/\omega_{cB}$ , and (b) normalized growth rate,  $\gamma/\omega_{cB}$  vs  $\lambda_B = \frac{k_{\perp}^2 v_B^2}{2\omega_{cB}^2}$  for  $N_B/N_e = 0.5$ ,  $\beta_i = 0.001$ ,  $\frac{k_{\parallel}}{k_{\perp}} = 0.01$ ,  $\kappa = 3, \infty$  and various values of  $S$  as listed on the curves.

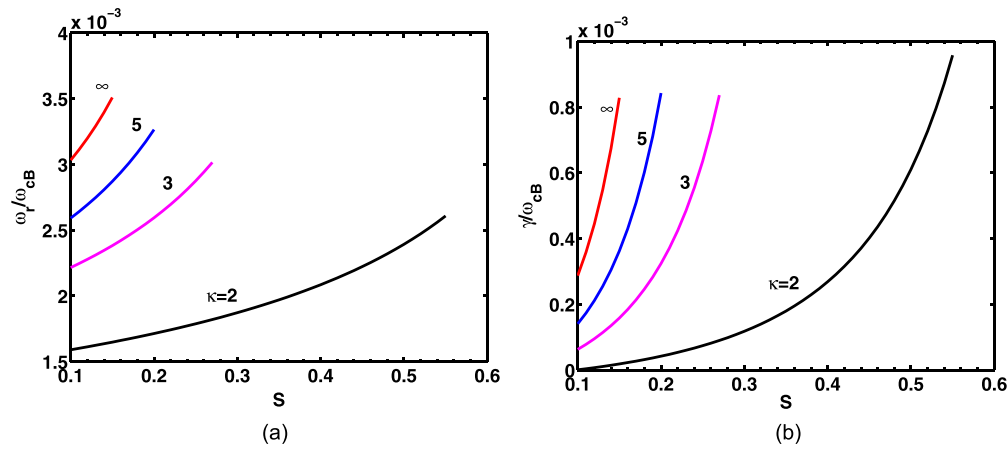


FIG. 4. KAW resonant instability driven by velocity shear: variation of (a) normalized real frequency,  $\omega_r/\omega_{cB}$ , and (b) normalized growth rate,  $\gamma/\omega_{cB}$  vs velocity shear  $S$  for  $N_B/N_e = 0.3$ ,  $\beta_i = 0.001$ ,  $k_{\parallel}/k_{\perp} = 0.01$ ,  $\lambda_B = 0.5$  and various values of  $\kappa$  as listed on the curves.

0.03 ( $\kappa = 3$ ), 0.02 ( $\kappa = 4$ ), and 0.017 for the Maxwellian electrons ( $\kappa = \infty$ ) for the parameters of Fig. 5.

Figure 6 shows the effect of propagation angle on the normalized real frequency and growth rate with  $\lambda_B$  for different  $k_{\parallel}/k_{\perp}$  values as indicated on the curves. For highly nonthermal electrons ( $\kappa = 3$ ), when  $k_{\parallel}/k_{\perp}$  increases the real frequency enhances, whereas the growth rate reduces. The largest growth rate is achieved at an angle of propagation close to  $90^\circ$ . Also the  $\lambda_B$  range for which these waves are excited gets restricted with the increase in  $k_{\parallel}/k_{\perp}$ . In the lower  $\lambda_B$  range, the change in real frequency is minimal for different  $k_{\parallel}/k_{\perp}$  values, whereas there is a significant change in the growth rate. On the other hand, in the higher  $\lambda_B$  region, the trend is different, i.e., there is a significant increase in the real frequency, whereas the change in the growth rate is minimal. It is observed that the real frequency is minimum for Maxwellian electrons ( $\kappa = \infty$ ), whereas the growth rate is maximum. It is also noticeable that for Maxwellian electrons the growth rate is achieved for a larger  $\lambda_B$  range. Our computations reveal that the wave growth is not possible beyond  $k_{\parallel}/k_{\perp} > 0.14$ , i.e.,

$\theta \leq 82^\circ$  for nonthermal electrons with  $\kappa = 3$ , whereas, for Maxwellian electrons, this limit is  $k_{\parallel}/k_{\perp} > 0.24$ , i.e.,  $\theta \leq 76.50^\circ$ . It can be inferred that Maxwellian electrons allow the wave to propagate far away from perpendicular propagation, whereas kappa electrons restrict the propagation of wave close to  $90^\circ$ .

Figure 7 delineates the variation of normalized real frequency and the growth rate with  $\lambda_B$  for different values of  $T_e/T_B$  as mentioned on the curves for nonthermal and Maxwellian electrons. Both real frequency and growth rate increase with the enhancement in  $T_e/T_B$ , and also the peak shifts toward the higher  $\lambda_B$ . It can be seen that with the increase in  $T_e/T_B$  the  $\lambda_B$  range for which the growth rate obtained also increases. The real frequency seems to flatten at larger values of  $T_e/T_B$ . It is inferred that a hot nonthermal electron favors the growth of KAWs. A Maxwellian electron can give a higher frequency and growth even at a smaller value of  $T_e/T_B$  as seen from the figure, and waves are excited for a larger  $\lambda_B$  range.

The variation of real frequency and growth rate with  $\lambda_B$  for different  $\beta_i$  is depicted in Fig. 8. The real frequency as well as the growth

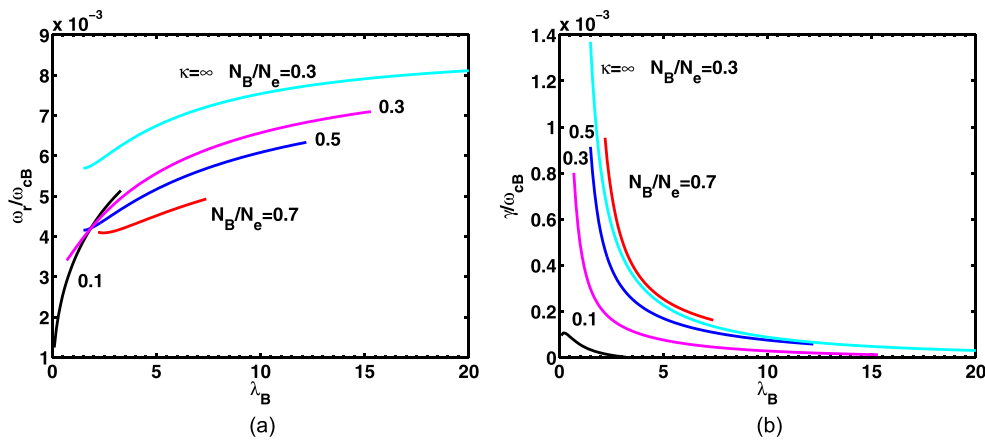


FIG. 5. KAW resonant instability driven by velocity shear: variation of (a) normalized real frequency,  $\omega_r/\omega_{cB}$ , and (b) normalized growth rate,  $\gamma/\omega_{cB}$  vs  $\lambda_B = \frac{k_{\perp}^2 \alpha_B^2}{2\omega_{cB}^2}$  for  $S = 0.3$ ,  $\kappa = (3, \infty)$ ,  $\beta_i = 0.001$ ,  $k_{\parallel}/k_{\perp} = 0.01$  and various values of  $N_B/N_e$  as listed on the curves.

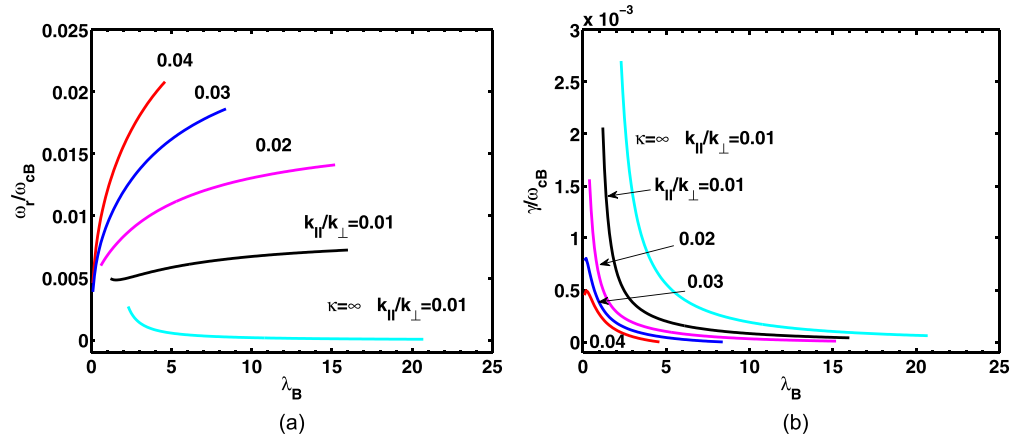


FIG. 6. KAW resonant instability driven by velocity shear: variation of (a) normalized real frequency,  $\omega_r/\omega_{cB}$ , and (b) normalized growth rate,  $\gamma/\omega_{cB}$  vs  $\lambda_B = \frac{k_{\perp}^2 \alpha_B^2}{2\omega_{cB}^2}$  for  $S = 0.5$ ,  $N_B = 0.3$ ,  $\beta_i = 0.001$ ,  $\kappa = 3, \infty$  and various values of  $k_{||}/k_{\perp}$  as listed on the curves.

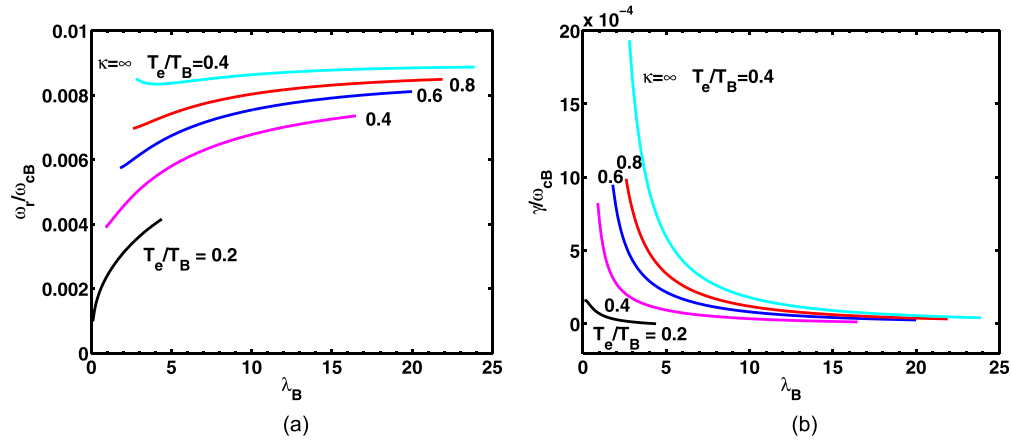


FIG. 7. KAW resonant instability driven by velocity shear: variation of (a) normalized real frequency,  $\omega_r/\omega_{cB}$ , and (b) normalized growth rate,  $\gamma/\omega_{cB}$  vs  $\lambda_B = \frac{k_{\perp}^2 \alpha_B^2}{2\omega_{cB}^2}$  for  $S = 0.3$ ,  $\kappa = 2, \infty$ ,  $N_B = 0.3$ ,  $k_{||}/k_{\perp} = 0.01$ ,  $\beta_i = 0.001$  and various values of  $T_e/T_B$  as listed on the curves.

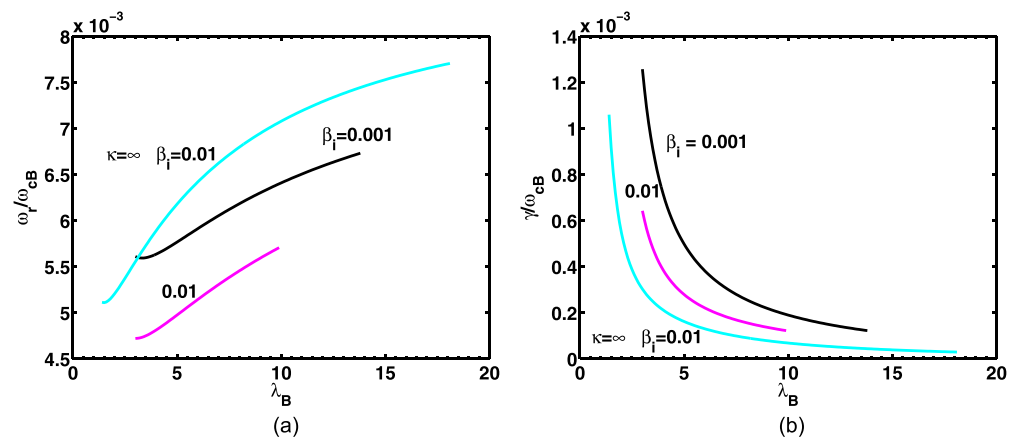


FIG. 8. KAW resonant instability driven by velocity shear: variation of (a) normalized real frequency,  $\omega_r/\omega_{cB}$ , and (b) normalized growth rate,  $\gamma/\omega_{cB}$  vs  $\lambda_B = \frac{k_{\perp}^2 \alpha_B^2}{2\omega_{cB}^2}$  for  $S = 0.5$ ,  $N_B = 0.5$ ,  $k_{||}/k_{\perp} = 0.01$ ,  $\kappa = 3, \infty$  and various values of  $\beta_i$ , as listed on the curves.

rate is maximum for a smaller  $\beta_i$ , and both decrease with the increase in  $\beta_i$ . The wave number ranges for which KAWs are excited decrease with the increase in  $\beta_i$  values. For a Maxwellian electron, the real frequency as well as wave number range increases and the growth rate decreases for fixed values of wavenumber and  $\beta_i$  in comparison with kappa electrons.

## V. RESULTS AND CONCLUSION

A theoretical model consisting of background Maxwellian ions, kappa electrons, and Maxwellian ion beams with a velocity shear is presented. The role played by nonthermal  $\kappa$  electrons in the excitation of KAWs is examined. It is seen that a small velocity shear can excite KAWs with Maxwellian electrons, whereas a very high velocity shear is required to excite KAWs when  $\kappa$  electrons are present. For a fixed set of parameters, for highly nonthermal electrons, a larger ion beam density is required to excite KAWs with the same growth rate as compared to Maxwellian electrons. The presence of kappa electrons has an adverse effect on the growth of KAWs and also it restricts the range of wave numbers for which KAWs are excited. It is also observed that a hot nonthermal electron favors the growth of KAWs rather than a cold one. The maximum growth rate is obtained for the KAWs propagating closer to the  $90^\circ$  wave normal angle. It is found that a Maxwellian electron allows the wave propagation at an angle far away from  $90^\circ$ , whereas a kappa electron restricts the wave to propagate at an angle closer to  $90^\circ$ .

We would like to point out that the obliquely propagating electrostatic ion waves can be excited by localized transverse electric fields in the presence of currents flowing along the magnetic field in a weakly collisional plasma.<sup>48,49</sup> Recently, inhomogeneous energy-density-driven instability (IEDDI) of electrostatic ion cyclotron waves have been studied both theoretically<sup>50</sup> and through numerical simulation.<sup>51</sup> The typical growth rate of the IEDDI of electrostatic ion cyclotron waves, normalized with respect to proton cyclotron frequency, is on the order of  $10^{-3}$ , whereas frequencies are on the order of  $0.6\Omega_p$ . In our case, we are exciting KAWs with much lower frequencies; however, growth rates are comparable to IEDDI of electrostatic ion cyclotron waves.<sup>50,51</sup> We must emphasize that the above electrostatic instabilities require the presence of a shear in the drift velocity component transverse to the magnetic field arising from the inhomogeneous transverse electric field. In our case, the KAW instability is driven by the shear in the drift velocity component parallel to the magnetic field. Furthermore, the shear in parallel drift velocity can also excite electrostatic low-frequency Kelvin-Helmholtz and ion cyclotron instabilities.<sup>23</sup>

The intense ion flows with  $V_B = 10^3$  km/s concentrated in a layer of thickness  $\sim 10^2$  to  $10^4$  km have been observed in the high-latitude plasma sheet boundary layer.<sup>52</sup> Considering a typical proton cyclotron frequency of  $\omega_{cB} \approx 0.4$  Hz gives the shear parameter  $S = (0.05-5)$ .<sup>23</sup> In polar cusp region at altitudes of  $5-7R_E$ , large ion flows ( $V_B/\alpha_B \leq 2$ ) with the gradient scale lengths,  $L_v \sim (100-200)$  km, have been observed.<sup>53</sup> Considering the typical proton cyclotron frequency  $\omega_{cB} \approx (2.2-3)$  Hz gives velocity shear  $S \approx (0.1-1.0)$ .<sup>23,24,27</sup> The observed ion beam densities in the polar cusp region are  $N_B/N_e = (0.01-0.2)$ .<sup>25,52,53</sup> For our numerics, we assume  $N_B/N_e = (0.1-0.7)$ ,  $\beta_i = (0.001-0.01)$  and  $S = (0.01-1.0)$ . Also, we consider the ion beam cyclotron frequency,  $\omega_{cB}/2\pi \approx (2.2-3.0)$  Hz, common at the auroral altitude of  $5-7R_E$ , the hot electron temperature,

$T_e \approx 100$  eV, the background cold ion temperature,  $T_i \approx 10$  eV, and the beam ion temperature,  $T_B \approx 1-2$  keV.

The maximum normalized growth rate and the corresponding real frequency for the resonant instability of KAWs excited by velocity shear in the presence of nonthermal electrons (Fig. 5, curve of  $N_B/N_e = 0.3, S = 0.3, \kappa = 3, \beta_i = 0.001, k_{\parallel}/k_{\perp} = 0.01$ ) are found as 0.0008 and 0.0034 at  $\lambda_B = 0.7$ . The respective un-normalized growth rate and real frequencies are given by 0.002 Hz and 0.0085 Hz, respectively. The velocity shear in the presence of a nonthermal electron can produce waves with frequencies in the range of 8.5–18 mHz and a growth rate of 0.3–2 mHz in the  $\lambda_B$  range of 0.7–15.3. The perpendicular wave number  $k_{\perp}$  can be found by using the formula  $k_{\perp} = \sqrt{2\lambda_B\omega_{cB}/\alpha_B}$  and is given as  $k_{\perp} \approx (0.03-0.14)$  km<sup>-1</sup>; the corresponding wavelength is in the range of 209–45 km. The parallel wave number can be obtained from the relation  $k_{\parallel}/k_{\perp} = 0.01$  and is found as  $(0.03-0.14) \times 10^{-2}$  km<sup>-1</sup> with the respective parallel wavelength as  $(209-45) \times 10^2$  km.

The typical growth time of the instability is  $\sim (500-1000)$  s. Since ion beams in the plasma sheet boundary layer last typically for  $\sim 1$  h, there is sufficient time for the instability to grow. Subsequently, the finite amplitude KAWs will transport their energy to the auroral region by propagating along the magnetic field lines.<sup>6,10,54</sup> Similarly, the KAW instability excited in the polar cusp at altitudes of  $5-7R_E$  can grow to significant amplitudes as ion beams have been observed very often on each pass of Hawkeye 1 and HEOS 2.<sup>53</sup>

The perpendicular wavelength value obtained from our model, i.e.,  $\lambda_{\perp} \approx (45-209)$  km, is in good agreement with the observed values of (20–120) km in the polar region.<sup>10</sup> Also, the parallel wavelength of  $\lambda_{\parallel} \approx (45-209) \times 10^2$  km predicted by our model matches very well with the observed value of (1000–10 000) km.<sup>10</sup> The three component plasma model can produce KAWs in the frequency range of  $\approx (8.5-18)$  mHz which may be helpful in understanding the properties of the observed ultralow-frequency (ULF) ( $\approx 1$  mHz–30 Hz)<sup>6,10,17,54,55</sup> magnetic turbulence at the auroral altitude.<sup>56</sup> The presence of  $\kappa$  electrons in our model may help to uncover some of the effects of non-thermal distribution in the magnetosphere.

## ACKNOWLEDGMENTS

G.S.L. thanks the Indian National Science Academy, New Delhi for the support under the INSA-Honorary Scientist Scheme.

## REFERENCES

- <sup>1</sup>B. J. Thompson and R. L. Lysak, *J. Geophys. Res.: Space Phys.* **101**, 5359–5369, <https://doi.org/10.1029/95JA03622> (1996).
- <sup>2</sup>C. H. Hui and C. E. Seyler, *J. Geophys. Res.* **97**, 3953, <https://doi.org/10.1029/91JA03101> (1992).
- <sup>3</sup>A. Hasegawa and L. Chen, *Phys. Fluids* **19**, 1924 (1976).
- <sup>4</sup>C. K. Goertz and R. W. Boswell, *J. Geophys. Res.* **84**, 7239, <https://doi.org/10.1029/JA084iA12p07239> (1979).
- <sup>5</sup>J. R. Johnson, C. Z. Cheng, and P. Song, *Geophys. Res. Lett.* **28**, 227–230, <https://doi.org/10.1029/2000GL012048> (2001).
- <sup>6</sup>C. C. Chaston, *J. Geophys. Res.* **110**, A02211, <https://doi.org/10.1029/2004JA010483> (2005).
- <sup>7</sup>M. H. Boehm, C. W. Carlson, J. P. McFadden, J. H. Clemmons, and F. S. Mozer, *J. Geophys. Res.* **95**, 12157, <https://doi.org/10.1029/JA095iA08p12157> (1990).
- <sup>8</sup>J.-E. Wahlund, P. Louarn, T. Chust, H. de Feraudy, A. Roux, B. Holback, P.-O. Dovner, and G. Holmgren, *Geophys. Res. Lett.* **21**, 1831–1834, <https://doi.org/10.1029/94GL01289> (1994).

- <sup>9</sup>P. Louarn, J. E. Wahlund, T. Chust, H. de Feraudy, A. Roux, B. Holback, P. O. Downer, A. I. Eriksson, and G. Holmgren, *Geophys. Res. Lett.* **21**, 1847–1850, <https://doi.org/10.1029/94GL00882> (1994).
- <sup>10</sup>J. R. Wygant, A. Keiling, C. A. Cattell, R. L. Lysak, M. Temerin, F. S. Mozer, C. A. Kletzing, J. D. Scudder, V. Streltsov, W. Lotko, and C. T. Russell, *J. Geophys. Res.: Space Phys.* **107**, SMP 24–1, <https://doi.org/10.1029/2001JA900113> (2002).
- <sup>11</sup>S. Duan, Z. Liu, and V. Angelopoulos, *Chin. Sci. Bull.* **57**, 1429–1435 (2012).
- <sup>12</sup>A. Keiling, J. R. Wygant, C. Cattell, M. Temerin, F. S. Mozer, C. A. Kletzing, J. Scudder, C. T. Russell, W. Lotko, and A. V. Streltsov, *Geophys. Res. Lett.* **27**, 3169–3172, <https://doi.org/10.1029/2000GL001127> (2000).
- <sup>13</sup>A. Keiling, *J. Geophys. Res.* **107**, SMP 24–1, <https://doi.org/10.1029/2001JA900140> (2002).
- <sup>14</sup>A. Keiling, G. K. Parks, J. R. Wygant, J. Dombeck, F. S. Mozer, C. T. Russell, A. V. Streltsov, and W. Lotko, *J. Geophys. Res.* **110**, A10S11, <https://doi.org/10.1029/2004JA010907> (2005).
- <sup>15</sup>A. Keiling, J. Wygant, C. Cattell, M. Johnson, M. Temerin, F. Mozer, C. Kletzing, J. Scudder, and C. Russell, *J. Geophys. Res.: Space Phys.* **106**, 5779–5798, <https://doi.org/10.1029/2000JA900130> (2001).
- <sup>16</sup>D. M. Malaspina, S. G. Claudepierre, K. Takahashi, A. N. Jaynes, S. R. Elkington, R. E. Ergun, J. R. Wygant, G. D. Reeves, and C. A. Kletzing, *Geophys. Res. Lett.* **42**, 9203–9212, <https://doi.org/10.1002/2015GL065935> (2015).
- <sup>17</sup>D. J. Gershman, A. F-Viñas, J. C. Dorelli, S. A. Boardsen, L. A. Avanov, P. M. Bellan, S. J. Schwartz, B. Lavraud, V. N. Coffey, M. O. Chandler, Y. Saito, W. R. Paterson, S. A. Fuselier, R. E. Ergun, R. J. Strangeway, C. T. Russell, B. L. Giles, C. J. Pollock, R. B. Torbert, and J. L. Burch, *Nat. Commun.* **8**, 14719 (2017).
- <sup>18</sup>N. D. Angelo, *J. Geophys. Res.* **78**, 1206–1209, <https://doi.org/10.1029/JA078i007p01206> (1973).
- <sup>19</sup>N. D. Angelo, *Rev. Geophys.* **15**, 299, <https://doi.org/10.1029/RG015i003p00299> (1977).
- <sup>20</sup>L. Chen and A. Hasegawa, *J. Geophys. Res.* **79**, 1024–1032, <https://doi.org/10.1029/JA079i007p01024> (1974).
- <sup>21</sup>J. Huba, *J. Geophys. Res.* **86**, 8991–9000, <https://doi.org/10.1029/JA086iA11p08991> (1981).
- <sup>22</sup>R. L. Lysak and C. T. Dum, *J. Geophys. Res.* **88**, 365, <https://doi.org/10.1029/JA088iA01p00365> (1983).
- <sup>23</sup>G. S. Lakhina, *J. Geophys. Res.* **92**, 12161, <https://doi.org/10.1029/JA092iA11p12161> (1987).
- <sup>24</sup>G. S. Lakhina, *Astrophys. Space Sci.* **165**, 153–161 (1990).
- <sup>25</sup>R. L. Lysak and W. Lotko, *J. Geophys. Res.: Space Phys.* **101**, 5085–5094, <https://doi.org/10.1029/95JA03712> (1996).
- <sup>26</sup>M. Nosé, T. Iyemori, M. Sugiura, J. Slavin, R. Hoffman, J. Winningham, and N. Sato, *J. Geophys. Res.: Space Phys.* **103**, 17587–17604, <https://doi.org/10.1029/98JA01187> (1998).
- <sup>27</sup>G. S. Lakhina, *Adv. Space Res.* **41**, 1688–1694 (2008).
- <sup>28</sup>K. C. Barik, S. V. Singh, and G. S. Lakhina, *Phys. Plasmas* **26**, 022901 (2019).
- <sup>29</sup>R. P. Sharma and K. V. Modi, *Phys. Plasmas* **20**, 082305 (2013).
- <sup>30</sup>R. P. Sharma, R. Goyal, E. E. Scime, and N. K. Dwivedi, *Phys. Plasmas* **21**, 042113 (2014).
- <sup>31</sup>K. V. Modi and R. P. Sharma, *Phys. Plasmas* **20**, 032303 (2013).
- <sup>32</sup>N. Yadav, R. K. Rai, P. Sharma, R. Uma, and R. P. Sharma, *Phys. Plasmas* **24**, 062902 (2017).
- <sup>33</sup>V. M. Vasyliunas, *J. Geophys. Res.* **73**, 7519–7523, <https://doi.org/10.1029/JA073i023p07519> (1968).
- <sup>34</sup>C. Pollock, J. Burch, A. Chasapis, B. Giles, D. Mackler, W. Matthaeus, and C. Russell, *J. Atmos. Terr. Phys.* **177**, 84–91 (2018).
- <sup>35</sup>R. F. Benson, A. F. Viñas, V. A. Osherovich, J. Fainberg, C. M. Purser, M. L. Adrian, I. A. Galkin, and B. W. Reinisch, *J. Geophys. Res.: Space Phys.* **118**, 5039–5049, <https://doi.org/10.1002/jgra.50459> (2013).
- <sup>36</sup>G. Livadiotis, *J. Geophys. Res.: Space Phys.* **120**, 880–903, <https://doi.org/10.1002/2014JA020671> (2015).
- <sup>37</sup>M. Lazar, H. Fichtner, and P. H. Yoon, *Astron. Astrophys.* **589**, A39 (2016).
- <sup>38</sup>K. Ogasawara, K. Asamura, T. Takashima, Y. Saito, and T. Mukai, *Earth Planets Space* **58**, 1155–1163 (2006).
- <sup>39</sup>D. Summers and R. M. Thorne, *Phys. Fluids B: Plasma Phys.* **3**, 1835–1847 (1991).
- <sup>40</sup>N. Rubab, N. V. Erkaev, and H. K. Biernat, *Phys. Plasmas* **16**, 103704 (2009).
- <sup>41</sup>N. Rubab, N. V. Erkaev, D. Langmayr, and H. K. Biernat, *Phys. Plasmas* **17**, 103704 (2010).
- <sup>42</sup>N. Rubab, V. Erkaev, H. K. Biernat, and D. Langmayr, *Phys. Plasmas* **18**, 073701 (2011).
- <sup>43</sup>B. Basu, *Phys. Plasmas* **16**, 052106 (2009).
- <sup>44</sup>A. Hasegawa, *J. Geophys. Res.* **81**, 5083–5090, <https://doi.org/10.1029/JA081i028p05083> (1976).
- <sup>45</sup>D. G. Swanson, *Plasma Waves (Series in Plasma Physics)* (CRC Press, 2003).
- <sup>46</sup>M. A. Hellberg and R. L. Mace, *Phys. Plasmas* **9**, 1495–1504 (2002).
- <sup>47</sup>I. A. Khan, Z. Iqbal, and G. Murtaza, *Eur. Phys. J. Plus* **134**, 80 (2019).
- <sup>48</sup>G. Ganguli, P. Palmadesso, and Y. C. Lee, *Geophys. Res. Lett.* **12**, 643–646, <https://doi.org/10.1029/GL012i010p00643> (1985).
- <sup>49</sup>G. Ganguli and P. J. Palmadesso, *Geophys. Res. Lett.* **15**, 103–106, <https://doi.org/10.1029/GL015i001p00103> (1988).
- <sup>50</sup>A. A. Chernyshov, A. A. Ilyasov, M. M. Mogilevskii, I. V. Golovchanskaya, and B. V. Kozelov, *Plasma Phys. Rep.* **41**, 254–261 (2015).
- <sup>51</sup>A. A. Ilyasov, A. A. Chernyshov, M. M. Mogilevskiy, I. V. Golovchanskaya, and B. V. Kozelov, *Phys. Plasmas* **22**, 032906 (2015).
- <sup>52</sup>G. K. Parks, M. McCarthy, R. J. Fitzenreiter, J. Etcheto, K. A. Anderson, R. R. Anderson, T. E. Eastman, L. A. Frank, D. A. Gurnett, C. Huang, R. P. Lin, A. T. Y. Lui, K. W. Ogilvie, A. Pedersen, H. Reme, and D. J. Williams, *J. Geophys. Res.* **89**, 8885, <https://doi.org/10.1029/JA089iA10p08885> (1984).
- <sup>53</sup>N. D. Angelo, A. Bahnsen, and H. Rosenbauer, *J. Geophys. Res.* **79**, 3129–3134, <https://doi.org/10.1029/JA079i022p03129> (1974).
- <sup>54</sup>J. R. Wygant, A. Keiling, C. A. Cattell, M. Johnson, R. L. Lysak, M. Temerin, F. S. Mozer, C. A. Kletzing, J. D. Scudder, W. Peterson, C. T. Russell, G. Parks, M. Brittner, G. Germany, and J. Spann, *J. Geophys. Res.: Space Phys.* **105**, 18675–18692, <https://doi.org/10.1029/1999JA900500> (2000).
- <sup>55</sup>C. C. Chaston, T. D. Phan, J. W. Bonnell, F. S. Mozer, M. Acuña, M. L. Goldstein, A. Balogh, M. Andre, H. Reme, and A. Fazakerley, *Phys. Rev. Lett.* **95**, 065002 (2005).
- <sup>56</sup>D. A. Gurnett and L. A. Frank, *J. Geophys. Res.* **83**, 1447, <https://doi.org/10.1029/JA083iA04p01447> (1978).